HHS Public Access

Author manuscript

J Bone Miner Res. Author manuscript; available in PMC 2015 May 01.

Published in final edited form as:

J Bone Miner Res. 2015 May ; 30(5): 824–836. doi:10.1002/jbmr.2420.

Pathophysiological role of vascular smooth muscle alkaline phosphatase in medial artery calcification†

Campbell R. Sheen, Ph.D.[1], **Pia Kuss, Ph.D.**[1], **Sonoko Narisawa, Ph.D.**[1], **Manisha C. Yadav, Ph.D.**[1], **Jessica Nigro, B.S.**[2], **Wei Wang, Ph.D.**[1], **T. Nicole Chhea, B.S.**[1], **Eduard A. Sergienko, Ph.D.**[3], **Kapil Kapoor, M.D., Ph.D.**[2], **Michael R. Jackson, Ph.D.**[3], **Marc. F. Hoylaerts, Ph.D.**[4], **Anthony B. Pinkerton, Ph.D.**[3], **W. Charles O'Neill, M.D.**[5], and **Jose Luis Millán, Ph.D.**[1]

[1]Sanford Children's Health Research Center, Sanford-Burnham Medical Research Institute, La Jolla, CA 92037

[2]Cardiometabolic Phenotyping Core, Sanford-Burnham Medical Research Institute at Lake Nona, Orlando, FL 32827

[3]Conrad Prebys Center for Chemical Genomics, Sanford-Burnham Medical Research Institute, La Jolla, CA 92037

[4]Department of Cardiovascular Sciences, Center for Molecular and Vascular Biology, University of Leuven, Leuven, Belgium

[5]Renal Division, Emory University School of Medicine, Atlanta, GA 30322

Abstract

Medial vascular calcification (MVC) is a pathological phenomenon common to a variety of conditions, including aging, chronic kidney disease, diabetes, obesity, and a variety of rare genetic diseases, that causes vascular stiffening and can lead to heart failure. These conditions share the common feature of tissue-nonspecific alkaline phosphatase (TNAP) upregulation in the vasculature. To evaluate the role of TNAP in MVC, we developed a mouse model that overexpresses human TNAP in vascular smooth muscle cells in an X-linked manner. Hemizygous overexpressor male mice (*Tagln-Cre*$^{+/-}$; *Hprt*$^{ALPL/Y}$, or TNAP-OE) show extensive vascular calcification, high blood pressure, cardiac hypertrophy and have a median age of death of 44 days, whereas the cardiovascular phenotype is much less pronounced and life expectancy is longer in heterozygous (*Tagln-Cre*$^{+/-}$; *Hprt*$^{ALPL/-}$) female TNAP-OE mice. Gene expression analysis showed upregulation of osteoblast and chondrocyte markers and decreased expression of vascular smooth muscle markers in the aortas of TNAP-OE mice. Through medicinal chemistry efforts, we

†This article has been accepted for publication and undergone full peer review but has not been through the copyediting, typesetting, pagination and proofreading process, which may lead to differences between this version and the Version of Record. Please cite this article as doi: [10.1002/jbmr.2420]

Correspondence Address: José Luis Millán, Ph.D., Sanford-Burnham Medical Research Institute, 10901 North Torrey Pines Road, La Jolla, CA 92037. Tel: +1-858-646-3130; Fax: +1-858-795-5381; millan@sanfordburnham.org.

Data on the medial calcification model was presented in part at the 34th Annual Meeting of the American Society for Bone and Mineral Research, October 12-15, 2012, Minneapolis, MN and efficacy data using SBI-425 was presented in part at the 35th Annual Meeting of the American Society for Bone and Mineral Research, October 4-7, 2013, Baltimore, MD.

Additional Supporting Information may be found in the online version of this article.

developed inhibitors of TNAP with drug-like pharmacokinetic characteristics. TNAP-OE mice were treated with the prototypical TNAP inhibitor SBI-425 or vehicle to evaluate the feasibility of TNAP inhibition *in vivo*. Treatment with this inhibitor significantly reduced aortic calcification and cardiac hypertrophy, and extended lifespan over vehicle-treated controls, in the absence of secondary effects on the skeleton. This study shows that TNAP in the vasculature contributes to the pathology of MVC and that it is a druggable target.

Keywords

genetic animal models; preclinical studies; matrix mineralization; therapeutics

Introduction

Calcification of vascular structures, which is associated with several diseases and conditions, independently predicts risk of cardiovascular events and mortality[1, 2] and has been called an imminent disease epidemic.[3] In particular, calcification of the elastic medial layers of the arterial system, known as medial vascular calcification (MVC), is commonly associated with aging[2, 4, 5], diabetes,[6] and chronic kidney disease (CKD),[7, 8] as well as variety of rare monogenic diseases,[9-11] and has been recognized as increasingly important contributor to cardiovascular disease.[4] MVC is distinct from the occlusive intimal calcification seen in atherosclerotic plaques, and has profound cardiovascular consequences. Arteries affected by MVC have reduced compliance and elastance,[5, 8] which increases pulse and systolic blood pressures, and cardiac workload. This leads to reduced coronary perfusion, left ventricular hypertrophy and remodeling, increased risk of myocardial infarction and heart failure. MVC is a strong independent predictor of cardiovascular mortality in end stage renal disease patients receiving hemodialysis[7] and is also associated with risk of amputation in type 2 diabetes patients.[6]

MVC was long thought to be a passive degenerative consequence of aging, but more recently has been recognized as a pathological consequence of imbalance between pro- and anti-calcific factors[12] and is an actively-regulated process that shares some mechanistic aspects with skeletal mineralization. Procalcific stimuli, including dysregulation of calcium and phosphate metabolism, inflammation, osteogenic gene expression and transdifferentiation by vascular smooth muscle cells (VSMCs) and nucleation by apoptotic bodies or matrix vesicles, are balanced by inhibitors such as extracellular pyrophosphate (PP_i), matrix Gla protein (MGP) and fetuin, which prevent spontaneous calcification of tissues.[12] Relaxation of this inhibition in bone is essential for normal skeletal development. However, depletion of these molecules in soft tissues, such as the vasculature, can cause pathological ectopic calcification.[9, 13, 14]

PP_i is an extremely potent inhibitor of calcification that binds to mineralizing surfaces to prevent crystal growth.[15] The extracellular levels of PP_i are regulated by the hydrolytic activity of the ectoenzyme tissue-nonspecific alkaline phosphatase (TNAP), encoded by the *ALPL* gene. TNAP is essential for normal skeletal development, as hypomorphic mutations

in *ALPL* lead to PP_i accumulation and defective mineralization in hypophosphatasia patients.[16] This defect is accurately reproduced in *Alpl* null mice[17, 18] and normalization of PP_i in these mice improves skeletal mineralization.[19, 20]

Despite its clear importance in the skeleton, the role of TNAP in MVC is still a topic of debate. There is a substantial body of indirect evidence linking TNAP upregulation and PP_i deficiency to MVC. TNAP upregulation has been observed in MVC associated with diabetes,[21] in patients undergoing dialysis[22, 23] and in arterial calcification due to CD73 deficiency (ACDC),[10] and has been proposed as a cause of the MVC seen in uremia.[24] TNAP upregulation is also seen in animal models of diabetic artery calcification,[25] renal failure,[24] Huntington-Gilford Progeria Syndrome (HGPS)[26] and MGP deficiency[27] and in vascular smooth muscle cells (VSMCs) isolated from *Enpp1*-knockout mice.[28, 29] The importance of PP_i in MVC is exemplified by the observation that humans and mice with deficient PP_i production, caused by defects in the enzyme responsible for PP_i synthesis from ATP (ectonucleotide pyrophosphatase/phosphodiesterase 1; ENPP1), exhibit severe MVC.[9, 30] Furthermore, PP_i administration to uremic rats or to mice with HGPS prevents MVC,[26, 31] and calcification of mouse *Enpp1* knockout VSMCs can be suppressed by chemical inhibitors of TNAP.[29] Thus, while TNAP expression clearly correlates with MVC, its contribution to the disease process is still uncertain. To evaluate the role of TNAP in MVC, we developed a mouse model of VSMC-specific overexpression of TNAP, which clearly shows that TNAP upregulation is sufficient to cause MVC. Furthermore, we developed a pharmacological inhibitor of TNAP, SBI-425, and show that long-term administration of SBI-425 effectively reaches and inhibits TNAP in the vasculature, improving cardiovascular parameters and survival at a dose that does not cause a detectable change in bone, demonstrating that vascular TNAP is a druggable target.

Materials and Methods

Animals and ethics statement

Tg(Tagln-cre)1Her mice[32, 33] expressing Cre recombinase under the control of the smooth muscle cell-specific *Tagln* promoter (*Tagln*-Cre, also known as *SM22*-Cre) were obtained from The Jackson Laboratory (Bar Harbor, ME, USA; stock 004746). Characterization of this transgenic mouse line has shown strong expression in the vascular media but not the endothelium during embryogenesis with some activity detected in the heart, but no expression elsewhere, including muscle cells in the stomach, gut, kidney, bladder, esophagus or in veins[32, 33]. $Hprt^{ALPL}$ knock-in mice were generated by GenOway (Lyon, France) using their proprietary “Quick Knock-in™” technology. This mouse strain has a construct containing the ubiquitous CAG promoter, a floxed “stop cassette” and the human *ALPL* cDNA inserted into the *Hprt* locus on the X chromosome (Fig. S1). The knock-in mice were developed using the E14Tg2a (E14) embryo-derived stem cells (ES) derived from the 129P2/OlaHsd (129Ola) mouse strain. The targeted insertion of TNAP-containing transgenic cassette using the “Quick Knock-in™” targeting vector repairs the Hprt gene deletion in E14 ES cells as this targeting vector rescues the expression of the endogenous *Hprt* gene. After transfection, the E14 ES cells with a functional *Hprt* gene were selected using HAT media to enrich for ES cell clones showing the correct targeting event.

Crossbreeding of the *Hprt*^{ALPL} mice with Cre-expressing animals results in excision of the stop cassette and transgene expression. Homozygous *Tagln-Cre* male mice were bred with homozygous female *Hprt*^{ALPL} mice to produce mice expressing TNAP in VSMCs. All offspring were either heterozygous *Tagln-Cre*$^{+/-}$; *Hprt*$^{ALPL/-}$ females (female TNAP-OE) or hemizygous *Tagln-Cre*$^{+/-}$; *Hprt*$^{ALPL/Y}$ males (male TNAP-OE). WT control mice on the same genetic background were generated by initially breeding TNAP-OE males and females together, then crossing their offspring to produce female *Tagln-Cre*$^{-/-}$; *Hprt*$^{-/-}$ and *Tagln-Cre*$^{-/-}$; *Hprt*$^{-/Y}$ male WT mice. Mice were genotyped by PCR using DNA extracted from tail clips using a Purelink Genomic DNA Mini kit (Invitrogen, Carlsbad, CA, USA). Primer sequences, product sizes and thermal cycling parameters are provided in Table S1. Mice were euthanized by either CO_2 inhalation or injection with Avertin (2.5% 2, 2, 2-tribromoethanol; Sigma Aldrich, St Louis, MO, USA). Animals were fed Teklad Global 18% Protein Rodent Diet (Harlan Laboratories, Indianapolis, IN, USA) *ad libitum*. All animal studies were approved by the Institutional Animal Care and Use Committees of Sanford-Burnham Medical Research Institute and complied with National Institutes of Health guidelines for humane treatment of laboratory animals.

Plasma analysis

Blood was collected by cardiac puncture, transferred into Microtainer tubes coated with lithium heparin (Becton, Dickinson & Co., Franklin Lakes, NJ, USA) and centrifuged at 3000 × *g* for 10 min to prepare plasma that was then stored at −80°C until analysis. Plasma alkaline phosphatase, phosphorus, calcium and blood urea nitrogen were measured using a VetScan Comprehensive Diagnostic Profile rotor (Abaxis, Union City, CA, USA). Plasma pyrophosphate was determined as previously described.[34, 35]

Histology

Tissue samples for histological analysis were fixed in 4% (w/v) paraformaldehyde (PFA) in phosphate buffered saline (PBS), with the exception of hearts for Masson's trichrome staining, which were fixed in Bouin's fixative. Aortas and hearts were embedded in Optimal Cutting Temperature compound (Tissue-Tek, Torrance, CA, USA) and paraffin, respectively. Hematoxylin and eosin, von Kossa, Alizarin red and Masson's trichrome staining were performed according to standard methods. Alkaline phosphatase activity was stained as described.[36] TUNEL staining for apoptotic cells was performed using an ApopTag Peroxidase *In Situ* Apoptosis Detection kit (Millipore, Billerica, MA, USA) according to the manufacturer's instructions.

Aortic calcification

X-ray images were obtained with an MX-20 Specimen Radiographic System (Faxitron X-ray Corp., Chicago, IL, USA). Mice fixed in 4% PFA/PBS were analyzed using microcomputed tomography (μCT) by Numira Biosciences (Salt Lake City, UT, USA) as previously described.[37] The section of the aorta from the arch to the bifurcation was dissected, cleaned of fat and blood and used for calcium quantification. Calcium deposited in aortas was leeched by incubation in 1 M HCl for 18 h at 37°C and the calcium concentration in the acid solution was quantified using a cresolphthalein complexone

assay.[38] Aortas were dried at 55°C for 18 h then weighed, and aortic calcium content was normalized to tissue dry weight. Preparation of aortic samples for expression analyses is described in the supplemental methods.

Cardiovascular analysis

Hemodynamic analysis was performed on P21 C57BL/6 (WT) and TNAP-OE mice as described in the Supplemental methods. Echocardiography was performed using a Vevo2100 imaging system (FUJIFILM Visual Sonics, Toronto, Canada) equipped with an ultrahigh frequency linear array solid state transducer (MS400-18-38MHz), as described in the supplemental material.

TNAP inhibitor

SBI-425 was dissolved in 100% DMSO, then diluted to a 1 mg/mL working solution containing 10% DMSO, 10% Tween-80 and 80% water. Vehicle solution for injections had SBI-425 omitted. Mice were intraperitoneally injected with SBI-425, or an equivalent volume of vehicle, once per day. In each litter, pups of each sex with randomly divided into two groups for administration of SBI-425 or vehicle. In trial 1, survival analysis was performed on male TNAP-OE mice treated with SBI-425 or vehicle from P7 until death. In trial 2, male TNAP-OE mice were injected with SBI-425 or vehicle from P7 to P16 or P30, at which time they were weighed and sacrificed. Hearts were dissected and weighed to calculate the heart weight to body weight ratio and skulls were dissected for dynamic histomorphometry, described below. Aortic calcification was quantified using the cresolphthalein complexone assay described above. In trial 3, female TNAP-OE mice were treated from P7 to P60, at which time heart weight to body weight ratio and aortic calcium deposition were measured as in Trial 2, and femora were used for static histomorphometry as described below. Static histomorphometry of femora was used to determine whether SBI-425 had any effects on bone volume. Skeletal preparation methods are described in the Supplement.

Statistical analysis

All numerical values are presented as the mean ± standard deviation (SD). Data were compared using a two-tailed Student's t-test or a nonparametric two-tailed Mann-Whitney test, as indicated. Survival curves were compared using the log-rank test. Analyses were performed with Prism v.6 software (GraphPad, La Jolla, CA, USA) and a *P*-value less than 0.05 was considered statistically significant.

Results

Overexpression of TNAP in VSMCs causes MVC—To test the hypothesis that upregulating TNAP in VSMCs would be sufficient to cause MVC, we generated a conditional knock-in mouse model that can overexpress TNAP in specific cell types via Cre-mediated expression of the knock-in transgene. A vector containing the human TNAP coding sequence under the control of the ubiquitous cytomegalovirus immediate early enhancer/chicken β-actin fusion promoter was produced (Fig. S1). This construct also included a loxP-flanked "stop cassette" between the promoter and transgene to prevent

overexpression in the absence of Cre recombinase. The transgenic construct was then introduced into the constitutively-active hypoxanthine phosphoribosyltransferase (*Hprt*) locus on the X chromosome. This mouse line, named $Hprt^{ALPL}$, was used to examine the effects of TNAP overexpression in VSMCs. Homozygous $Hprt^{ALPL/ALPL}$ female mice were bred with male mice expressing Cre-recombinase under the control of the VSMC-specific transgelin promoter (*Tagln-Cre*).[32, 33] By breeding $Tagln\text{-}Cre^{+/+}$ males with $Hprt^{ALPL/ALPL}$ homozygous females, all male offspring are hemizygous $Hprt^{ALPL/Y}$; $Tagln\text{-}Cre^{+/-}$ (hereafter referred to as male TNAP-OE mice) and expected to display a full overexpression phenotype. Because of the X-linked nature of this transgene and the variability introduced by X-chromosome inactivation, heterozygous $Hprt^{ALPL/-}$; $Tagln\text{-}Cre^{+/-}$ female mice (hereafter referred to as female TNAP-OE mice) were expected to show a milder phenotype.

Plasma alkaline phosphatase activity was 4-fold higher in hemizygous male TNAP-OE mice than in WT at 14 days of age and 22-fold higher than WT at 30 days of age (Fig. 1A). In contrast female TNAP-OE mice only reached about 12-fold increase in serum TNAP activity at 150 days of age (Fig. 1A). Aortic calcium was measured in acid extracts from aortas by the o-cresolphthalein complexone colorimetric assay (Fig. 1B), which showed that male TNAP-OE mice had significantly higher aortic calcium content that female TNAP-OE mice at P14 and P30 ($P<0.0001$ by two-tailed t-test). Female TNAP-OE aortas reached levels of calcium deposition comparable to P30 male TNAP-OE aortas at P60 (Fig. 1B). Microcomputed tomography of a P30 male TNAP-OE mouse showed massive arterial calcification in the ascending and descending aorta, and the left and right carotid and subclavian arteries (Fig. 1C). While arterial calcification was not detected by X-ray imaging in P7 TNAP-OE mice, it was visible in the aorta at P14 and was extensive at P30 in male TNAP-OE mice (Fig. 1D). A comparative sagittal view of whole mount Alizarin red staining of P14 male and P14 female TNAP-OE aortas are shown in Fig. 1D. Even though TNAP-OE mice displayed significantly higher plasma alkaline phosphatase activity at P14 and P30 than WT controls (approximately 4- and 18-fold, respectively; both $P<0.001$ by two-tailed t-test), there was no significant difference in the plasma concentration of PP_i between the plasma of WT and TNAP-OE mice at P14 ($P>0.05$ by two-tailed t-test) and no systemic differences in phosphorus and calcium concentrations (Table 1 & Table S3).

The effect of TNAP overexpression on vascular histology was assessed in aortas from P7, P14 and P30 TNAP-OE mice (Fig. 2) Alkaline phosphatase activity was confined to the vascular media and was observed at all ages in TNAP-OE mice, but not in age-matched WTs. Alizarin red and von Kossa staining showed no visible deposits of calcium or phosphate, respectively, at P7. However, calcification had developed by P14 and became more extensive at P30, consistent with X-ray analysis. No calcium or phosphate deposition was detected in WT controls. Because transdifferentiation of VSMCs to osteogenic cells is a common feature of MVC, we analyzed gene expression patterns to look for evidence of this process in TNAP-OE mice. The relative expression of genes involved in tissue mineralization in aortas collected at P14 and P30 showed a clear pattern of chondro-osteogenesis (Table 2). Expression of genes for the canonical markers of MVC osteopontin (*Spp1*), bone morphogenetic protein 2 (*Bmp2*), matrix gla protein (*Mgp*), and endogenous mouse tissue-nonspecific alkaline phosphatase (*Alpl*) was significantly higher in TNAP-OE

males than in WT at both P14 and P30 (Table 2). Expression of *Runx2*, a marker of early osteoblastic differentiation was higher in TNAP-OE than WT at both P14 and P30, whereas the later osteoblastic gene *Col1a1*, was only upregulated at P30. Similarly, the early marker of chondrocyte differentiation, *Sox9*, was upregulated in TNAP-OE at both ages, whereas the later chondrocyte marker *Acan* was upregulated at P30 only. The genes for the vascular smooth muscle proteins α-smooth muscle actin (*Acta2*) and transgelin (*Tagln*) were downregulated in TNAP-OE males at P30, but not at P14. Expression of the gene for the phosphate importer Pit1 (*Slc20a1*) was higher in TNAP-OE than WT males at both ages, and expression of the gene for the PP_i-producing protein ectonucleotide pyrophosphatase/phosphodiesterase 1 (*Enpp1*) was higher than WT at P30, whereas expression of the PP_i-exporter ankylosis (*Ank*) gene was unchanged at both ages.

Cardiovascular phenotype in TNAP-OE mice—We next determined whether the MVC in TNAP-OE mice has an effect on cardiovascular function. Litter size and pre-weaning mortality of male and female TNAP-OE mice were not significantly different from WT controls ($P>0.05$ by two-tailed t-test for both parameters).

However, male TNAP-OE mice experienced pronounced early mortality, with a median age of death of 44 days and all mice dying before approximately 5 months of age (range 25-142 days) (Fig. 3A), which was significantly different from WT ($P<0.0001$ by log-rank test). Mice died suddenly, with no overt signs of illness or loss of weight. Male TNAP-OE mice manifested substantial cardiac enlargement (Fig. 3B), beginning as early as P14. This worsened with age, to the point that the mean heart weight to body weight ratio (HW:BW) was approximately two and three times that of WT at P30 and P49, respectively (Fig. 3C). Hemodynamic assessment was performed in P21 male TNAP-OE mice, a time point where the mice where large enough for catheterization and their degree of calcification was not as pronounced as to prevent catheter insertion. Systolic blood pressure was significantly higher than WT in TNAP-OE mice ($P<0.0001$ by two-tailed t-test), as was pulse pressure ($P<0.0001$) (Fig. 3D). No differences in diastolic pressure were observed. Further analysis of the structural and functional parameters of P21 male TNAP-OE and WT mice was performed by M-mode echocardiography (Table 3). The calculated left ventricular mass showed left ventricular hypertrophy in all groups of TNAP-OE mice, consistent with HW:BW measurements. Several structural parameters, including left ventricular wall thickness at diastole, interventricular septum distance and relative wall thickness were also higher than WT in the TNAP-OE group. No differences in end-diastolic or end-systolic volumes were observed between genotypes. Notably, ejection fraction was significantly lower in male P21 TNAP-OE mice than in WT, indicating functional impairment of the heart. Apoptotic cells in histological sections were detected by terminal deoxynucleotidyl transferase dUTP nick end labeling (TUNEL) in P49 mice (Fig. 3E), which showed the proportion of apoptotic cells in TNAP-OE mice was significantly higher than in WT mice ($P<0.001$ by two-tailed t-test) (Fig. 3F), indicating ventricular remodeling. Masson's trichrome staining of P49 male hearts showed extensive interstitial collagen deposition, indicative of fibrosis, in TNAP-OE mice that was not observed in WT counterparts (Fig. 3G). HE staining of a 49-day-old male heart showed severe hypertrophy of the left ventricle and the left atrial appendage, which may be consistent with atrial fibrillation (Fig. 3H).

These changes in cardiac structure and function are consistent with pressure overload-induced hypertrophy and progression to heart failure.

As expected from the X-linked nature of this model, female mice showed a much milder phenotype than male TNAP-OE mice. There was no difference in survival between female TNAP-OE and WT mice at 180 d ($p>0.05$ by log-rank test), but the mortality rate in female TNAP-OE mice increased after approximately 210 d and a significant difference in survival was observed at 1 year ($p<0.05$ by log-rank test). The median survival for female TNAP-OE mice was 296 d (Fig. 4A). There was a significant difference in survival between male and female TNAP-OE mice ($p<0.0001$ by log-rank test). No significant difference in heart weight vs body weight was observed between WT and TNAP-OE female mice at P30 (Fig. 4B). However, cardiac hypertrophy developed later in life. Fig. 4C shows X-ray images of the calcification of the aortic arch in a P57 male and a P323 female heart. Hemodynamic assessment was also performed in P21 female TNAP-OE mice. Systolic blood pressure was significantly higher in female TNAP-OE mice ($p<0.0001$) compared to WT mice, as was pulse pressure ($p<0.0001$) (Fig. 4D). No differences in diastolic pressure were observed. Analysis of the structural and functional parameters of P28 and P56 female TNAP-OE and WT mice was performed by echocardiogram in m-mode (Table 4). The calculated left ventricular mass index showed left ventricular hypertrophy in female TNAP-OE mice. Left ventricular wall thickness at diastole, interventricular septum distance and relative wall thickness were also higher than WT in female TNAP-OE mice. Stroke volume, cardiac output and left ventricular internal diameter at diastole were all lower in TNAP-OE than in WT P56 female mice (Table 4).

Development of a pharmacological inhibitor of TNAP—Given that overexpression of TNAP in VSMCs was sufficient to cause MVC, we next aimed to test the hypothesis that pharmacological inhibition of MVC-associated high TNAP activity would be feasible. We undertook a lead optimization campaign starting from a previously-identified chemical inhibitor of TNAP, MLS0038949 (here referred to as ML038),[39] with the goal of improving its pharmacokinetic properties, as per the strategy outlined in Fig. 5A. Numerous analogs were synthesized examining all areas of ML038 including the linker (in brown), dimethoxyphenyl group (in grey) and quinoline (in green). An iterative structure-activity-relationship campaign led to several series of potent, selective and drug like leads. The compound we disclose herein, SBI-425 is a prototypical example from these efforts [40]. SBI-425 is a low nM (IC_{50}= 14 nM) TNAP inhibitor with no *in vitro* cross-inhibition of placental, intestinal or germ-cell alkaline phosphatases at concentrations up to 80 μM, or of the 35 proteins in the HitProfilingScreen + CYP450 panel, including the five major cytochrome P450 enzymes and the human potassium voltage-gated channel, subfamily H (eag-related), member 2 protein (hERG), at 10 μM.

SBI-425 was administered to C56B1/6J mice to analyze its pharmacokinetic properties. SBI-425 showed high plasma levels after intravenous (2 mg/kg) and oral (10 mg/kg) dosing (Fig. 5B), with sustained plasma levels >1 μM for over 12 h, greater than the *in vitro* IC_{90} for TNAP. Similar plasma levels were obtained at 2, 4 and 8 h in a cohort injected intraperitoneally. After oral and intravenous dosing, TNAP activity in plasma was inhibited at >90% for over 8 hours and at >50% over 24 h (Fig. 5C) at the same doses. Other key

pharmacokinetic parameters are shown in Table S4. These combined parameters showed that SBI-425 is a potent inhibitor of TNAP with drug-like pharmacokinetic properties.

To evaluate the ability of SBI-425 to target and inhibit TNAP in vascular smooth muscle cells, we performed three proof-of-concept trials. In all trials, TNAP-OE animals were treated once daily with vehicle or 10 mg/kg SBI-425. In Trial 1, TNAP-OE mice were treated from P7 until death. SBI-425 treatment significantly prolonged the lifespan of TNAP-OE mice; the median age of death for the vehicle-treated group was 44 days (range 25–78 days) versus 68 days (range 43–156 days) in the SBI-425-treated group (Fig. 6A). In Trial 2, TNAP-OE mice were treated from P7 to P16 or P30, and aortic calcium content (Fig. 6B) and HW:BW (Fig. 6C) were measured. Aortic calcium was approximately 44% lower in the SBI-425-treatment group than the vehicle group at P16 ($P<0.05$ by two-tailed Mann-Whitney test), but no significant difference was observed at P30 ($P>0.05$ by two-tailed Mann-Whitney test). HW:BW was approximately 16% lower in the SBI-425 treatment group at P30 ($P<0.05$ by two-tailed Mann-Whitney test). No significant differences in body weight were observed in this trial. In Trial 3, we examined the effect of SBI-425 on double heterozygous $Hprt^{ALPL/Y}$; $Tagln\text{-}Cre^{+/-}$ female mice, which display a milder phenotype than males, and whose medial survival is 296 days. These female OE mice were treated from P7 to P60. Aortic calcium content (Fig. 6D) and HW:BW (Fig. 6E) were approximately 40% and 32%, respectively, lower in the SBI-425 treatment group than in the vehicle group ($P<0.05$ and $P<0.01$, respectively, by two-tailed Mann-Whitney test). No mice in either treatment group died during this trial, nor were there any significant differences in body weight. To determine whether SBI-425 treatment might cause deleterious effects on the skeleton, bone volume, osteoid volume and growth rate were measured by histomorphometry in P60 females (Trial 3; Fig. 6F and 6G) and by Alizarin red/calcein chase in P30 males (Trial 2; Fig. 6H). No significant differences between SBI-425 and vehicle treatment were observed in any of these parameters, indicating that SBI-425 did not cause functionally significant inhibition of TNAP in bone at a dose that improved vascular calcification, heart size and survival in TNAP-OE mice.

Discussion

TNAP-OE mice manifest extensive MVC early in life, in the absence of systemic changes in calcium, phosphate, or renal function. Expression of TNAP was confined to the medial layer of the vasculature in TNAP-OE mice, which showed calcium phosphate deposition that became more extensive with age. TNAP-OE mice showed progressive cardiac hypertrophy most likely secondary to systolic hypertension, cardiac fibrosis and ventricular remodeling, reduced ejection fraction and early mortality. These data clearly show that a selective rise of TNAP expression in the vasculature suffices to trigger MVC in the absence of the metabolic dysfunctions seen in CKD and diabetes.

The phenotype of TNAP-OE male mice closely resembles that seen in patients with generalized arterial calcification of infancy (GACI), a human disease which is caused by mutations in *ENPP1*, the gene that encodes the major enzyme that generates extracellular PP_i.[9] However, TNAP-OE mice do not exhibit a significant decrease in circulating PP_i levels, despite high levels of the circulating enzyme, which is consistent with other

transgenic models of tissue-specific TNAP expression.[37] This can be explained by the fact that, unlike genetic disorders where the gene is defective in all tissues and thus plasma PP_i reflects whole-body PP_i metabolism, TNAP-OE mice have a tissue-specific (smooth muscle cell-specific) increase in the enzyme. In addition, TNAP in the blood is not very active as it is largely inhibited by the physiological concentrations of inorganic phosphate.[41] Our data point to the sinking of extracellular PP_i concentrations in the medial microenvironment causing calcification in this model rather than changes in systemic levels. Measuring local extracellular PP_i concentrations in the heavily calcified segments of the

TNAP OE aortas has proven technically challenging. Nevertheless, the importance of context-specific TNAP activity has been clearly demonstrated in hypophosphatasia. Normalization of systemic TNAP levels in hypophosphatasia patients does not correct their symptoms,[42, 43] whereas administration of a mineral-targeted recombinant TNAP dramatically improves the disease in both humans and mice, presumably because of local correction of PP_i concentrations at sites of calcification.[16, 20] Results from TNAP-OE mice suggest a similar such requirement for localized activity in MVC and supports a model in which membrane-bound TNAP hydrolyzes PP_i in the vascular microenvironment enabling soft-tissue calcification.

It has been postulated that MVC is a cell-driven process - that is, osteogenic transdifferentiation occurs first and this causes the media to calcify.[21-23] Analysis of gene expression showed that relative expression of MVC and bone-type markers increased with age, whereas VSMC markers decreased, suggesting that PP_i depletion caused by TNAP overexpression can cause a transition of VSMCs to a mineralizing-type cell. In particular, the master osteogenic regulators *Bmp2* and *Runx2*, which are essential for osteochondrogenic reprogramming,[44] were upregulated, as were the mineralization inhibitors *Spp1* and *Mgp*, which may be an adaptive response to compensate for the loss of PP_i and limit pathological mineralization.[45] We also observed that overexpression of transgenic human TNAP induced upregulation of endogenous mouse *Alpl*, presumably due to transdifferentiation. Expression from the *Tagln* promoter used in this study begins in the vasculature as early as embryonic day 9,[32] suggesting that TNAP expression and thus PP_i depletion occur well in advance of the first signs of MVC in TNAP-OE mice. As expression levels of some markers of bone-type cells were already elevated at P14, the age at which we first observed calcification, it appears that both physiochemical and gene expression changes are involved in calcification. The extracellular ratio of P_i:PP_i has been proposed as an important controller of calcification[46, 47] but how the cells sense a change in this ratio is still unknown. High extracellular phosphate has been shown to induced expression of the phosphate transporter P_it1 in cultured VSMCs, which increases uptake of intracellular phosphate, inducing *Runx2* expression and osteogenic transdifferentiation of VSMCs.[48] However, MVC can occur in the absence of hyperphosphatemia in GACI, diabetes and aging, and we observed no hyperphosphatemia in TNAP-OE mice. Sage et al. showed that the calcium phosphate nanocrystals were responsible for signalling osteogenic differentiation.[49] Consistent with this, Villa-Bellosta et al. showed that the passive calcium phosphate deposition, that occurs under normal phosphate levels but only in the absence of calcification inhibitors, such as PP_i, signals the VSMC to express bone-type genes.[50, 51]

Thus, it is conceivable that the change in gene expression profile in TNAP-OE mice, consistent with transdifferentiation of VSMCs, is caused by local depletion of PP_i, and the consequent imbalance in the P_i:PP_i ratio, which allows deposition of calcium phosphate nanocrystals.

The extremely high potency of PP_i as an inhibitor of calcification makes it an attractive candidate for prevention or treatment of MVC.[47, 52, 53] O'Neill et al.[31] showed that PP_i administration to uremic rats can prevent or reduce MVC, without any overt effects on bone or calcium pyrophosphate deposition disease. Similarly, Villa-Bellosta et al.[26] demonstrated that PP_i administration in a mouse model of HGPS prevented vascular calcification. Despite the promise of PP_i administration, it is rapidly cleared,[31, 54] which precludes its clinical use. Bisphosphonates, non-hydrolysable analogues of PP_i, have been used to treat MVC in GACI[55] and CKD.[56, 57] However, the doses required can have deleterious effects on the skeleton.[58] An alternative approach to increase PP_i levels is to inhibit PP_i degradation by TNAP. In contrast to the short half-life of PP_i, TNAP inhibitors can be engineered to provide sustained inhibition of TNAP and augmentation of PP_i levels. Specific TNAP inhibitors previously identified by our group lower calcification in *Enpp1*-knockout mouse VSMCs and inhibit PP_i hydrolysis and calcification in *ex vivo* rat aortas.[29, 51] To build on the promise of PP_i modulation by TNAP inhibitors, we optimized one of the molecules identified during a high-throughput screen for specific TNAP inhibitors[39, 59] by SAR to produce a derivative with drug-like properties, SBI-425.

The use of TNAP inhibitors to modulate PP_i concentrations for the treatment of MVC would also require that such compounds engage TNAP in the vasculature, rather than inhibiting TNAP in the circulation alone. We observed that administration of SBI-425 significantly reduced aortic calcium deposition, heart size and prolongation of life in TNAP-OE mice thus reversing the physiological consequences caused by the specific genetic upregulation of TNAP in the vasculature. Importantly, that benefit was achieved with an SBI-425 dose that did not adversely affect bone mineralization. This outcome is consistent with a study demonstrating that PP_i administration to uremic rats reduced MVC without overt effects on bone.[31]

The dose of SBI-425 used in this proof-of-concept study was not expected nor intended to completely arrest calcification as the level of TNAP expression in TNAP-OE mice vastly exceeds that commonly seen in MVC, no doubt contributing to the extreme severity of the phenotype in our genetic model. Pharmacological studies showed that a single daily i.p. injection of 10 mg/kg SBI-425 only inhibits plasma TNAP by approximately half, 24 h after dosing. As the degree of TNAP expression in TNAP-OE mice is supraphysiological, even reducing TNAP activity in the vasculature by half is not expected to be sufficient to completely arrest the process. Nevertheless, our data show that even modest reductions in cardiac hypertrophy and slowing of calcification can improve the physiological outcomes of MVC, which is consistent with London et al.,[60] who showed that regression of hypertrophy improves cardiovascular mortality in end-stage renal disease. An area in which TNAP inhibitors may be of most use is in the expanding catalogue of rare genetic disorders that are caused by PP_i dysregulation, GACI, ACDC, HGPS and pseudoxanthoma elasticum all manifest MVC as a result of dysfunctions in PP_i metabolism.

Supplementary Material

Refer to Web version on PubMed Central for supplementary material.

Acknowledgments

We thank Diana Sandoval from the Animal Facility at SBMRI La Jolla for her help with animal breeding and injections. We also thank John Shelley of the Histology Core Facility at SBMRI Lake Nona, and the staff of the Histopathology Core Facility at SBMRI La Jolla. CRS, KK, MRJ, EAS, MFH, WCO, ABP and JLM designed the studies. CRS, PK, SN, MCY, JN, KK, WW, TNC and ES performed the experiments. CRS, PK, SN, MCY, TCN, JN, KK, EAS and JLM analyzed the data. CRS, KK, ABP, WCO and JLM wrote the manuscript.

Grant support: This work was supported in part by grants X01MH077602, RC1HL101899, DE012889 and AG045933 from the National Institutes of Health, USA. CRS is the recipient of an American Heart Association Postdoctoral Fellowship. PK is the recipient of a Research Fellowship from the German Research Foundation (DFG).

References

1. Blacher J, Guerin AP, Pannier B, Marchais SJ, London GM. Arterial calcifications, arterial stiffness, and cardiovascular risk in end-stage renal disease. Hypertension. 2001; 38(4):938–42. [PubMed: 11641313]
2. Witteman JC, Kok FJ, van Saase JL, Valkenburg HA. Aortic calcification as a predictor of cardiovascular mortality. Lancet. 1986; 2(8516):1120–2. [PubMed: 2877272]
3. Towler DA. Vascular calcification: A perspective on an imminent disease epidemic. IBMS BoneKEy. 2008; 5(2):41–58.
4. Towler DA, Demer LL. Thematic series on the pathobiology of vascular calcification: an introduction. Circ Res. 2011; 108(11):1378–80. [PubMed: 21617134]
5. McEniery CM, McDonnell BJ, So A, et al. Aortic calcification is associated with aortic stiffness and isolated systolic hypertension in healthy individuals. Hypertension. 2009; 53(3):524–31. [PubMed: 19171791]
6. Lehto S, Niskanen L, Suhonen M, Ronnemaa T, Laakso M. Medial artery calcification. A neglected harbinger of cardiovascular complications in non-insulin-dependent diabetes mellitus. Arterioscler Thromb Vasc Biol. 1996; 16(8):978–83. [PubMed: 8696962]
7. London GM, Guerin AP, Marchais SJ, et al. Arterial media calcification in end-stage renal disease: impact on all-cause and cardiovascular mortality. Nephrol Dial Transplant. 2003; 18(9):1731–40. [PubMed: 12937218]
8. Sutliff RL, Walp ER, El-Ali AM, et al. Effect of medial calcification on vascular function in uremia. Am J Physiol Renal Physiol. 2011; 301(1):F78–83. [PubMed: 21478480]
9. Rutsch F, Ruf N, Vaingankar S, et al. Mutations in ENPP1 are associated with ‘idiopathic’ infantile arterial calcification. Nat Genet. 2003; 34(4):379–81. [PubMed: 12881724]
10. St Hilaire C, Ziegler SG, Markello TC, et al. NT5E mutations and arterial calcifications. N Engl J Med. 2011; 364(5):432–42. [PubMed: 21288095]
11. Nitschke Y, Rutsch F. Generalized arterial calcification of infancy and pseudoxanthoma elasticum: two sides of the same coin. Front Genet. 2012; 3:302. [PubMed: 23269929]
12. Sallam T, Cheng H, Demer LL, Tintut Y. Regulatory circuits controlling vascular cell calcification. Cell Mol Life Sci. 2013; 70(17):3187–97. [PubMed: 23269436]
13. El-Maadawy S, Kaartinen MT, Schinke T, et al. Cartilage formation and calcification in arteries of mice lacking matrix Gla protein. Connect Tissue Res. 2003; 44(Suppl 1):272–8. [PubMed: 12952208]
14. Schafer C, Heiss A, Schwarz A, et al. The serum protein alpha 2-Heremans-Schmid glycoprotein/fetuin-A is a systemically acting inhibitor of ectopic calcification. J Clin Invest. 2003; 112(3):357–66. [PubMed: 12897203]
15. Meyer JL. Can biological calcification occur in the presence of pyrophosphate? Arch Biochem Biophys. 1984; 231(1):1–8. [PubMed: 6326671]

16. Whyte MP, Greenberg CR, Salman NJ, et al. Enzyme-replacement therapy in life-threatening hypophosphatasia. N Engl J Med. 2012; 366(10):904–13. [PubMed: 22397652]
17. Narisawa S, Frohlander N, Millan JL. Inactivation of two mouse alkaline phosphatase genes and establishment of a model of infantile hypophosphatasia. Dev Dyn. 1997; 208(3):432–46. [PubMed: 9056646]
18. Fedde KN, Blair L, Silverstein J, et al. Alkaline phosphatase knock-out mice recapitulate the metabolic and skeletal defects of infantile hypophosphatasia. J Bone Miner Res. 1999; 14(12): 2015–26. [PubMed: 10620060]
19. Hessle L, Johnson KA, Anderson HC, et al. Tissue-nonspecific alkaline phosphatase and plasma cell membrane glycoprotein-1 are central antagonistic regulators of bone mineralization. Proc Natl Acad Sci U S A. 2002; 99(14):9445–9. [PubMed: 12082181]
20. Millan JL, Narisawa S, Lemire I, et al. Enzyme replacement therapy for murine hypophosphatasia. J Bone Miner Res. 2008; 23(6):777–87. [PubMed: 18086009]
21. Shanahan CM, Cary NR, Salisbury JR, et al. Medial localization of mineralization-regulating proteins in association with Monckeberg's sclerosis: evidence for smooth muscle cell-mediated vascular calcification. Circulation. 1999; 100(21):2168–76. [PubMed: 10571976]
22. Moe SM, Duan D, Doehle BP, O'Neill KD, Chen NX. Uremia induces the osteoblast differentiation factor Cbfa1 in human blood vessels. Kidney Int. 2003; 63(3):1003–11. [PubMed: 12631081]
23. Shroff RC, McNair R, Figg N, et al. Dialysis accelerates medial vascular calcification in part by triggering smooth muscle cell apoptosis. Circulation. 2008; 118(17):1748–57. [PubMed: 18838561]
24. Lomashvili KA, Garg P, Narisawa S, Millan JL, O'Neill WC. Upregulation of alkaline phosphatase and pyrophosphate hydrolysis: potential mechanism for uremic vascular calcification. Kidney Int. 2008; 73(9):1024–30. [PubMed: 18288101]
25. Ren X, Wei Q, Shao H, Sun Z, Liu N. A rat model of diabetic artery calcification. J Endocrinol Invest. 2012; 35(5):497–503. [PubMed: 21750399]
26. Villa-Bellosta R, Rivera-Torres J, Osorio FG, et al. Defective extracellular pyrophosphate metabolism promotes vascular calcification in a mouse model of Hutchinson-Gilford progeria syndrome that is ameliorated on pyrophosphate treatment. Circulation. 2013; 127(24):2442–51. [PubMed: 23690466]
27. Leroux-Berger M, Queguiner I, Maciel TT, et al. Pathologic calcification of adult vascular smooth muscle cells differs on their crest or mesodermal embryonic origin. J Bone Miner Res. 2011; 26(7):1543–53. [PubMed: 21425330]
28. Johnson K, Polewski M, van Etten D, Terkeltaub R. Chondrogenesis mediated by PPi depletion promotes spontaneous aortic calcification in NPP1-/- mice. Arterioscler Thromb Vasc Biol. 2005; 25(4):686–91. [PubMed: 15625282]
29. Narisawa S, Harmey D, Yadav MC, et al. Novel inhibitors of alkaline phosphatase suppress vascular smooth muscle cell calcification. J Bone Miner Res. 2007; 22(11):1700–10. [PubMed: 17638573]
30. Rutsch F, Vaingankar S, Johnson K, et al. PC-1 nucleoside triphosphate pyrophosphohydrolase deficiency in idiopathic infantile arterial calcification. Am J Pathol. 2001; 158(2):543–54. [PubMed: 11159191]
31. O'Neill WC, Lomashvili KA, Malluche HH, Faugere MC, Riser BL. Treatment with pyrophosphate inhibits uremic vascular calcification. Kidney Int. 2011; 79(5):512–7. [PubMed: 21124302]
32. Li L, Miano JM, Cserjesi P, Olson EN. SM22 alpha, a marker of adult smooth muscle, is expressed in multiple myogenic lineages during embryogenesis. Circ Res. 1996; 78(2):188–95. [PubMed: 8575061]
33. Holtwick R, Gotthardt M, Skryabin B, et al. Smooth muscle-selective deletion of guanylyl cyclase-A prevents the acute but not chronic effects of ANP on blood pressure. Proc Natl Acad Sci U S A. 2002; 99(10):7142–7. [PubMed: 11997476]

34. Johnson K, Vaingankar S, Chen Y, et al. Differential mechanisms of inorganic pyrophosphate production by plasma cell membrane glycoprotein-1 and B10 in chondrocytes. Arthritis Rheum. 1999; 42(9):1986–97. [PubMed: 10513816]
35. Yadav MC, Huesa C, Narisawa S, et al. Ablation of Osteopontin Improves the Skeletal Phenotype of Phospho1 Mice. J Bone Miner Res. 2014
36. Narisawa S, Hofmann MC, Ziomek CA, Millan JL. Embryonic alkaline phosphatase is expressed at M-phase in the spermatogenic lineage of the mouse. Development. 1992; 116(1):159–65. [PubMed: 1483384]
37. Narisawa S, Yadav MC, Millan JL. In vivo overexpression of tissue-nonspecific alkaline phosphatase increases skeletal mineralization and affects the phosphorylation status of osteopontin. J Bone Miner Res. 2013; 28(7):1587–98. [PubMed: 23427088]
38. Moorehead WR, Biggs HG. 2-Amino-2-methyl-1-propanol as the alkalizing agent in an improved continuous-flow cresolphthalein complexone procedure for calcium in serum. Clin Chem. 1974; 20(11):1458–60. [PubMed: 4421368]
39. Dahl R, Sergienko EA, Su Y, et al. Discovery and validation of a series of aryl sulfonamides as selective inhibitors of tissue-nonspecific alkaline phosphatase (TNAP). J Med Chem. 2009; 52(21):6919–25. [PubMed: 19821572]
40. Pinkerton AB, Dahl R, Cosford NDP, Millan JL. Inventors. Sulfonamide compounds and uses as tnap inhibitors. WO2013126608 A1. Feb 21.2013
41. Coburn SP, Mahuren JD, Jain M, Zubovic Y, Wortsman J. Alkaline phosphatase (EC 3.1.3.1) in serum is inhibited by physiological concentrations of inorganic phosphate. J Clin Endocrinol Metab. 1998; 83(11):3951–7. [PubMed: 9814474]
42. Whyte MP, Valdes R Jr, Ryan LM, McAlister WH. Infantile hypophosphatasia: enzyme replacement therapy by intravenous infusion of alkaline phosphatase-rich plasma from patients with Paget bone disease. J Pediatr. 1982; 101(3):379–86. [PubMed: 7108657]
43. Whyte MP, McAlister WH, Patton LS, et al. Enzyme replacement therapy for infantile hypophosphatasia attempted by intravenous infusions of alkaline phosphatase-rich Paget plasma: results in three additional patients. J Pediatr. 1984; 105(6):926–33. [PubMed: 6502342]
44. Speer MY, Li X, Hiremath PG, Giachelli CM. Runx2/Cbfa1, but not loss of myocardin, is required for smooth muscle cell lineage reprogramming toward osteochondrogenesis. J Cell Biochem. 2010; 110(4):935–47. [PubMed: 20564193]
45. Proudfoot D, Shanahan CM. Nanocrystals seed calcification in more ways than one. Kidney Int. 2011; 79(4):379–82. [PubMed: 21278777]
46. Murshed M, Harmey D, Millan JL, McKee MD, Karsenty G. Unique coexpression in osteoblasts of broadly expressed genes accounts for the spatial restriction of ECM mineralization to bone. Genes Dev. 2005; 19(9):1093–104. [PubMed: 15833911]
47. Persy VP, McKee MD. Prevention of vascular calcification: is pyrophosphate therapy a solution? Kidney Int. 2011; 79(5):490–3. [PubMed: 21321558]
48. Li L, Blumenthal DK, Masaki T, Terry CM, Cheung AK. Differential effects of imatinib on PDGF-induced proliferation and PDGF receptor signaling in human arterial and venous smooth muscle cells. J Cell Biochem. 2006; 99(6):1553–63. [PubMed: 16817200]
49. Sage AP, Lu J, Tintut Y, Demer LL. Hyperphosphatemia-induced nanocrystals upregulate the expression of bone morphogenetic protein-2 and osteopontin genes in mouse smooth muscle cells in vitro. Kidney Int. 2011; 79(4):414–22. [PubMed: 20944546]
50. Villa-Bellosta R, Wang X, Millan JL, Dubyak GR, O'Neill WC. Extracellular pyrophosphate metabolism and calcification in vascular smooth muscle. Am J Physiol Heart Circ Physiol. 2011; 301(1):H61–8. [PubMed: 21490328]
51. Villa-Bellosta R, Millan A, Sorribas V. Role of calcium-phosphate deposition in vascular smooth muscle cell calcification. Am J Physiol Cell Physiol. 2011; 300(1):C210–20. [PubMed: 20881235]
52. Towler DA. Inorganic pyrophosphate: a paracrine regulator of vascular calcification and smooth muscle phenotype. Arterioscler Thromb Vasc Biol. 2005; 25(4):651–4. [PubMed: 15790939]
53. O'Neill WC. Treatment of vascular calcification. Kidney Int. 2008; 74(11):1376–8. [PubMed: 19008909]

54. Jung A, Russel RG, Bisaz S, Morgan DB, Fleisch H. Fate of intravenously injected pyrophosphate-32P in dogs. Am J Physiol. 1970; 218(6):1757–64. [PubMed: 4317203]

55. Rutsch F, Boyer P, Nitschke Y, et al. Hypophosphatemia, hyperphosphaturia, and bisphosphonate treatment are associated with survival beyond infancy in generalized arterial calcification of infancy. Circ Cardiovasc Genet. 2008; 1(2):133–40. [PubMed: 20016754]

56. Lomashvili KA, Monier-Faugere MC, Wang X, Malluche HH, O'Neill WC. Effect of bisphosphonates on vascular calcification and bone metabolism in experimental renal failure. Kidney Int. 2009; 75(6):617–25. [PubMed: 19129793]

57. Toussaint ND, Elder GJ, Kerr PG. Bisphosphonates in chronic kidney disease; balancing potential benefits and adverse effects on bone and soft tissue. Clin J Am Soc Nephrol. 2009; 4(1):221–33. [PubMed: 18987295]

58. Otero JE, Gottesman GS, McAlister WH, et al. Severe skeletal toxicity from protracted etidronate therapy for generalized arterial calcification of infancy. J Bone Miner Res. 2013; 28(2):419–30. [PubMed: 22972716]

59. Sergienko E, Su Y, Chan X, et al. Identification and characterization of novel tissue-nonspecific alkaline phosphatase inhibitors with diverse modes of action. J Biomol Screen. 2009; 14(7):824–37. [PubMed: 19556612]

60. London GM, Pannier B, Guerin AP, et al. Alterations of left ventricular hypertrophy in and survival of patients receiving hemodialysis: follow-up of an interventional study. J Am Soc Nephrol. 2001; 12(12):2759–67. [PubMed: 11729246]

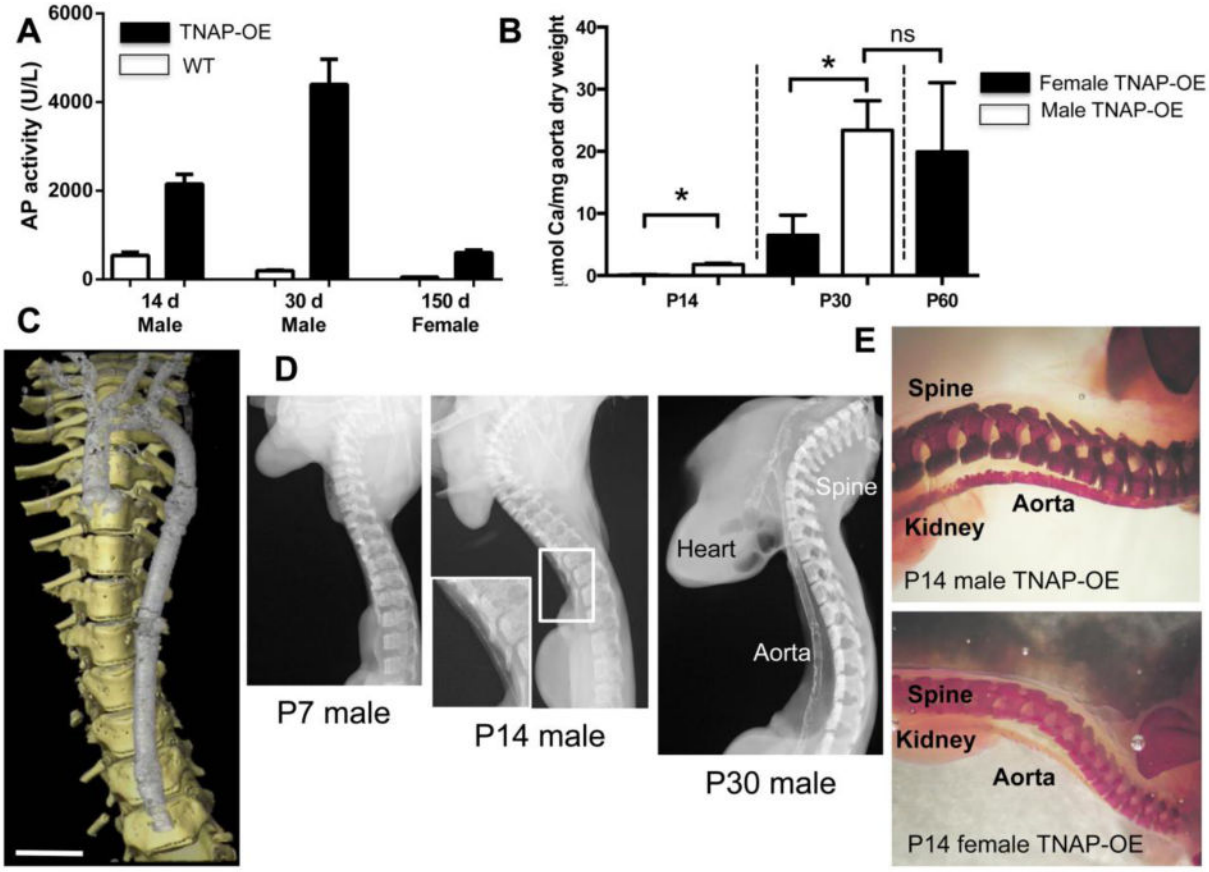

Fig. 1. Alkaline phosphatase activity and vascular calcification in TNAP-OE mice

(A) Plasma alkaline phosphatase activity in male TNAP-OE mice at 14 and 30 days and of female TNAP-OE mice at 150 days of life **(B)** Left side of the graph: Quantification of aortic calcium deposition in P14 male TNAP-OE mice compared to WT mice. Right side of the graph: quantification of aortic calcium in male and female aortas at P30 and P60. * denotes $P<0.001$, respectively, by two-tailed t-test ($N\geq3$). **(C)** Frontal view of microcomputed tomography imaging of a P30 TNAP-OE mouse. Calcification of the aorta and carotid and subclavian arteries is visible. Vascular and skeletal calcification are shown in white and yellow, respectively. Scale bar denotes 2 mm. **(D)** X-ray images showing sagittal view of TNAP-OE mice at P7, P14 and P30. Calcification is not visible at P7, faint at P14 (see inset) and extensive at P30. **(E)** Von Kossa staining of P14 male and female aortas.

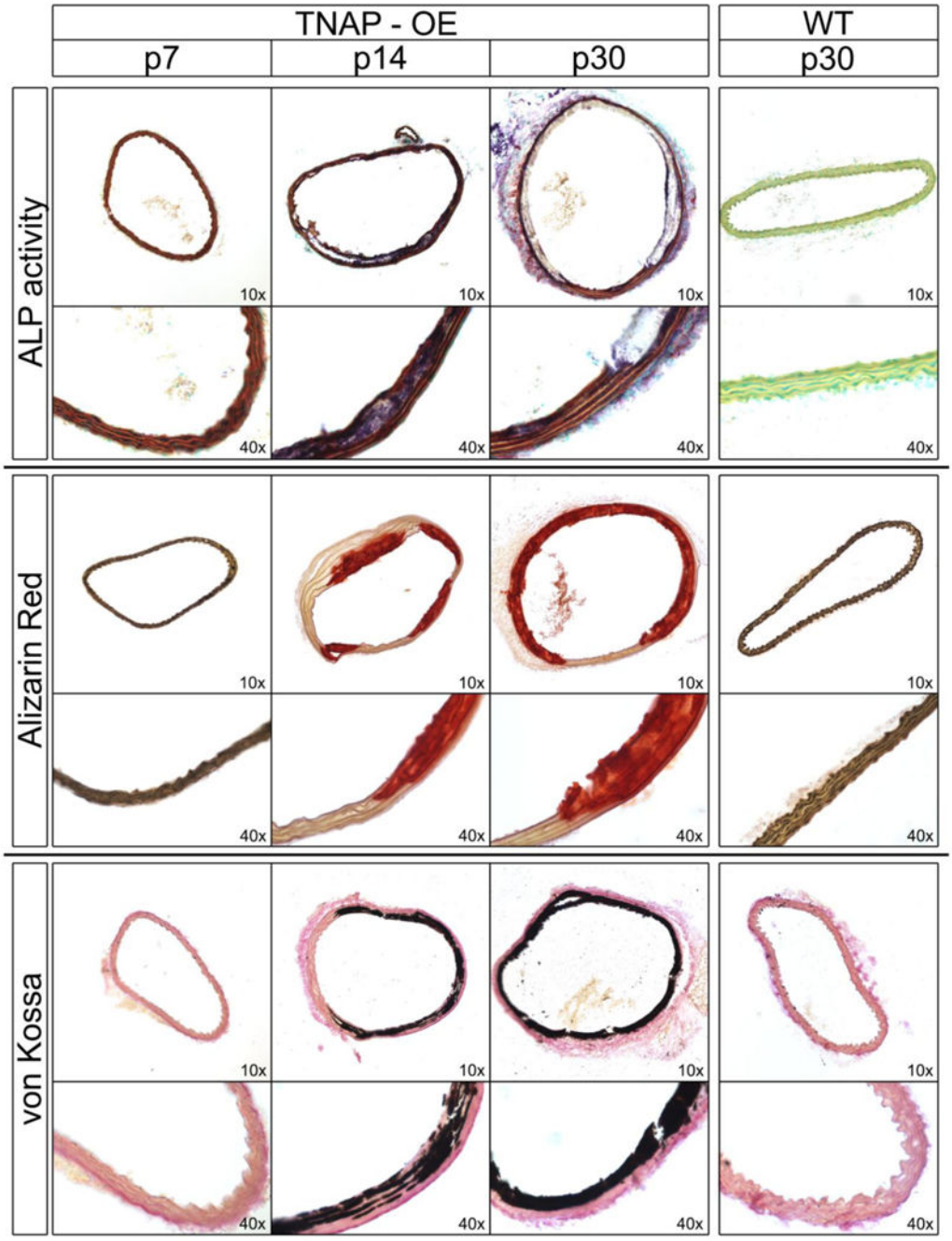

Fig. 2. Histological analysis of male TNAP-OE and WT aortas

Alkaline phosphatase (ALP) expression precedes vascular calcification in TNAP-OE mice. Neither alkaline phosphatase activity nor vascular calcification are observed in WT controls.

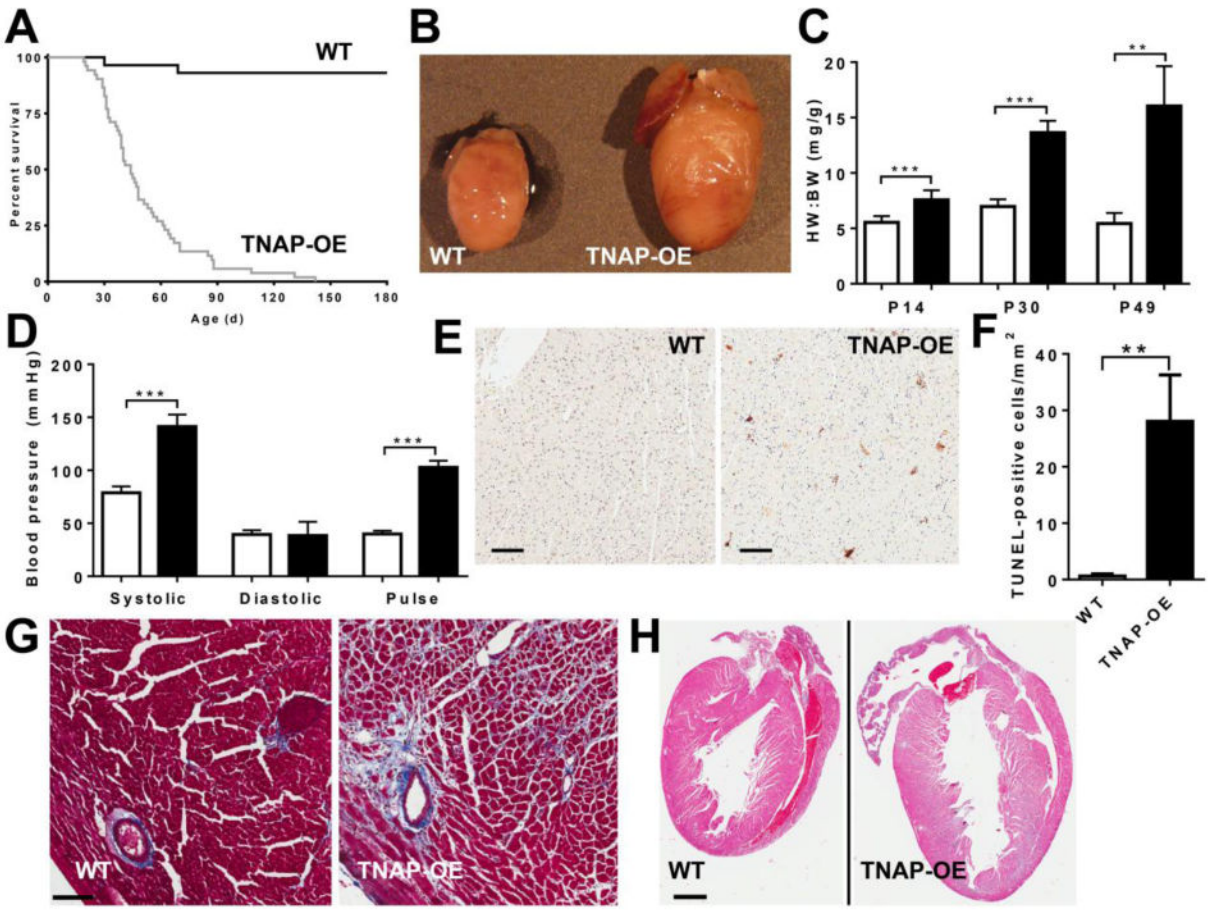

Fig. 3. Cardiac phenotype of male TNAP-OE mice

(A) Survival of male TNAP-OE mice is lower than WT counterparts ($P<0.0001$ by log-rank test). Black and grey lines represent WT and TNAP-OE genotypes, respectively. **(B)** Comparison of heart size in P30 male TNAP-OE and WT mice. Scale bar denotes 5 mm. **(C)** Comparison of heart weight to body weight ratio (HW:BW) between TNAP-OE and WT mice ($N\geq5$). **(D)** Hemodynamic measurements of TNAP-OE and WT mice at P21. Male TNAP-OE mice have significantly higher systolic and pulse pressures, whereas diastolic pressure is not different ($N\geq6$). **(E)** Images of TUNEL staining in ventricular sections of male TNAP OE mice and WT mice **(F)** Left ventricular apoptosis in WT and male TNAP-OE mice at P49 measured by TUNEL-staining. The increased incidence of apoptosis is consistent with ventricular remodeling ($N=3$ per group). **(G)** Masson's trichrome staining of left ventricle from WT (left) and TNAP-OE (right) mice at P49. Muscle fibers and collagen fibers are stained red and blue, respectively. TNAP-OE hearts display extensive interstitial and perivascular fibrosis. Scale bar denotes 100 μm. **(H)** Hematoxylin and eosin staining of coronal sections of hearts from WT (left) and TNAP-OE (right) mice at P49. LV denoted left ventricle and LAA denotes left atrial appendage. In all panels, black and white bars denote WT and TNAP-OE genotypes, respectively. *, ** and *** denote significance with $P<0.05$, $P<0.01$ and $P<0.001$, respectively, by two-tailed t-test.

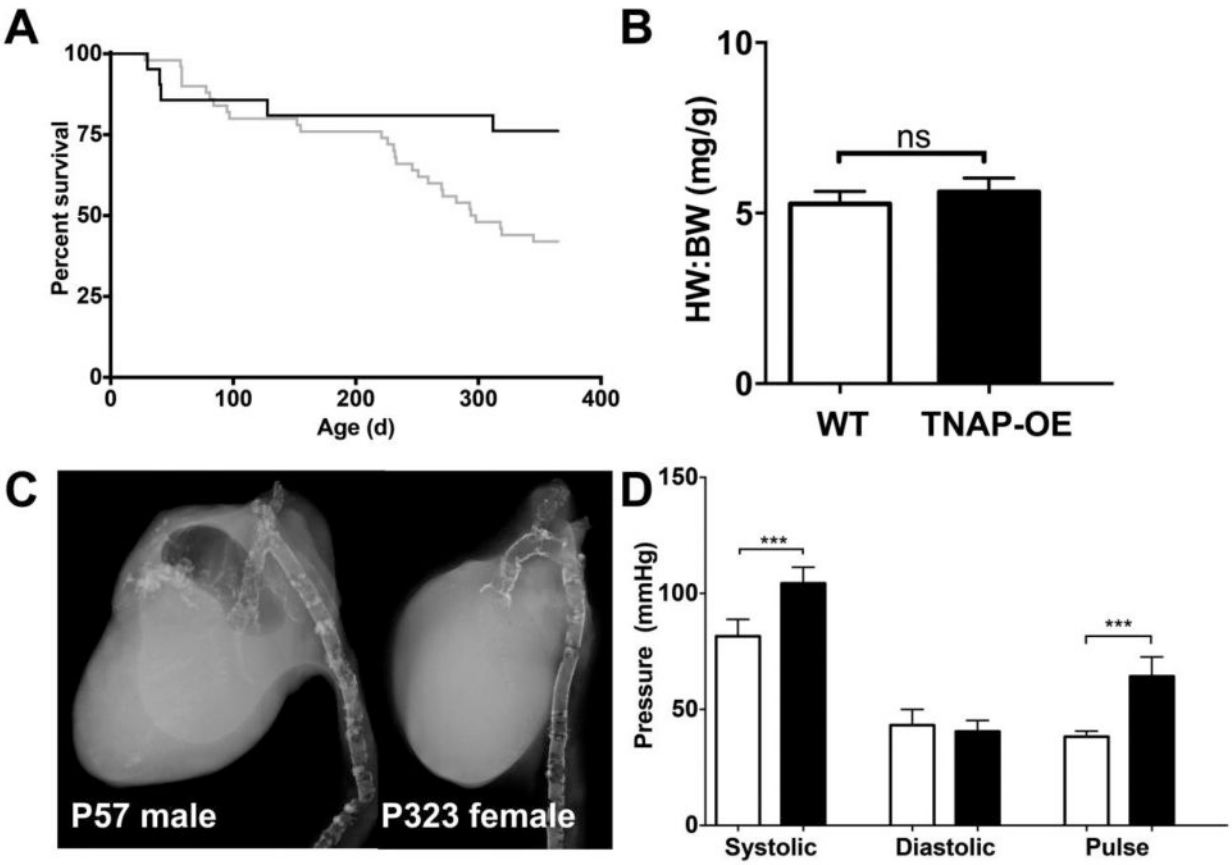

Fig. 4. Cardiac phenotype of female TNAP-OE mice

(A) Survival of female TNAP-OE mice is lower than WT counterparts ($P<0.0001$ by log-rank test). Black and grey lines represent WT and TNAP-OE genotypes, respectively. **(B)** Comparison of heart weight to body weight ratio (HW:BW) between TNAP-OE and WT mice ($N\geq5$). **(C)** X-ray images showing sagittal view of male and female TNAP-OE mice at P57 and P323, respectively. (D) Hemodynamic measurements of female TNAP-OE and WT mice at P21. Female TNAP-OE mice have significantly higher systolic and pulse pressures, whereas diastolic pressure is not different ($N\geq6$).

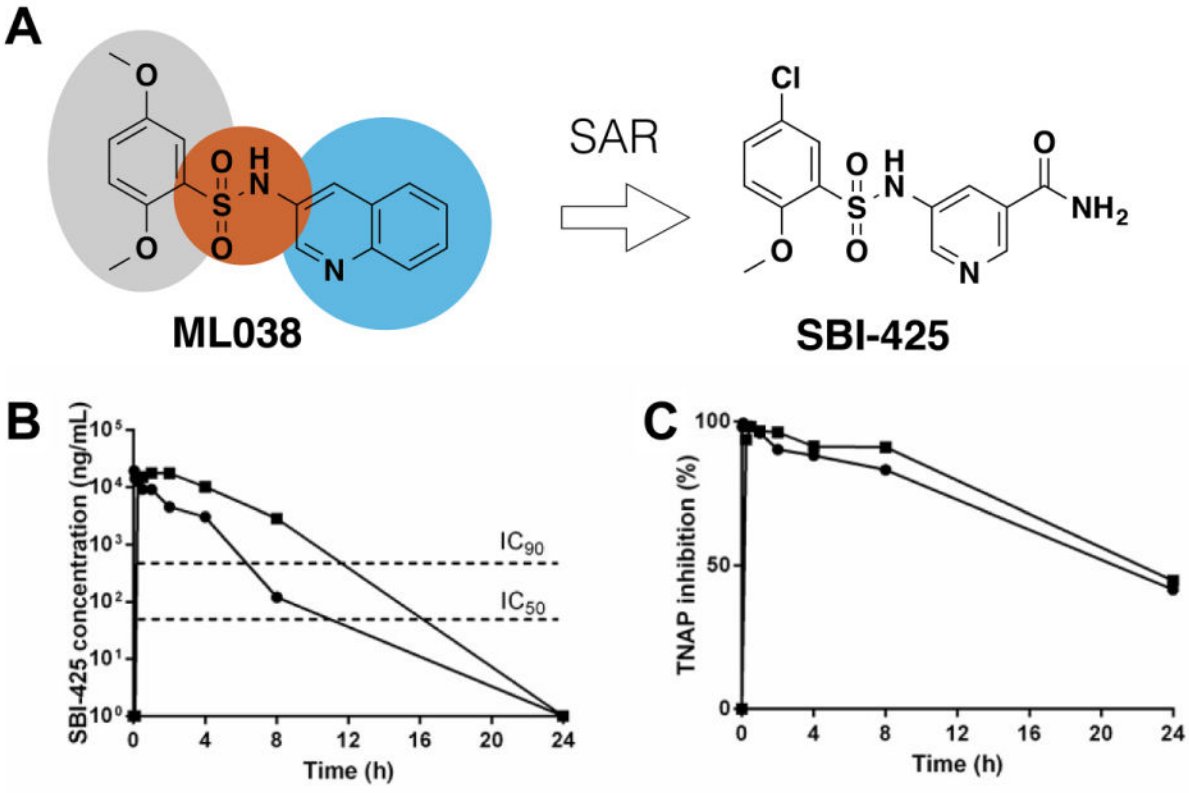

Fig. 5. Structure and pharmacokinetics of the TNAP inhibitor, SBI-425

(A) Structure of the MLS0038949 lead compound obtained by high throughput screening[39] and visualization of the linker (in brown), dimethoxyphenyl group (in grey) and quinoline (in green) moieties that were modified in iterative structure-activity-relashionship (SAR) efforts to obtain the SBI-425 inhibitor. **(B)** Plasma concentrations of SBI-425 and **(C)** inhibition of plasma TNAP activity by a single oral (square) or intravenous (circle) dose of SBI-425. The *in vitro* IC_{50} and IC_{90} of SBI-425 are indicated in **(B)**.

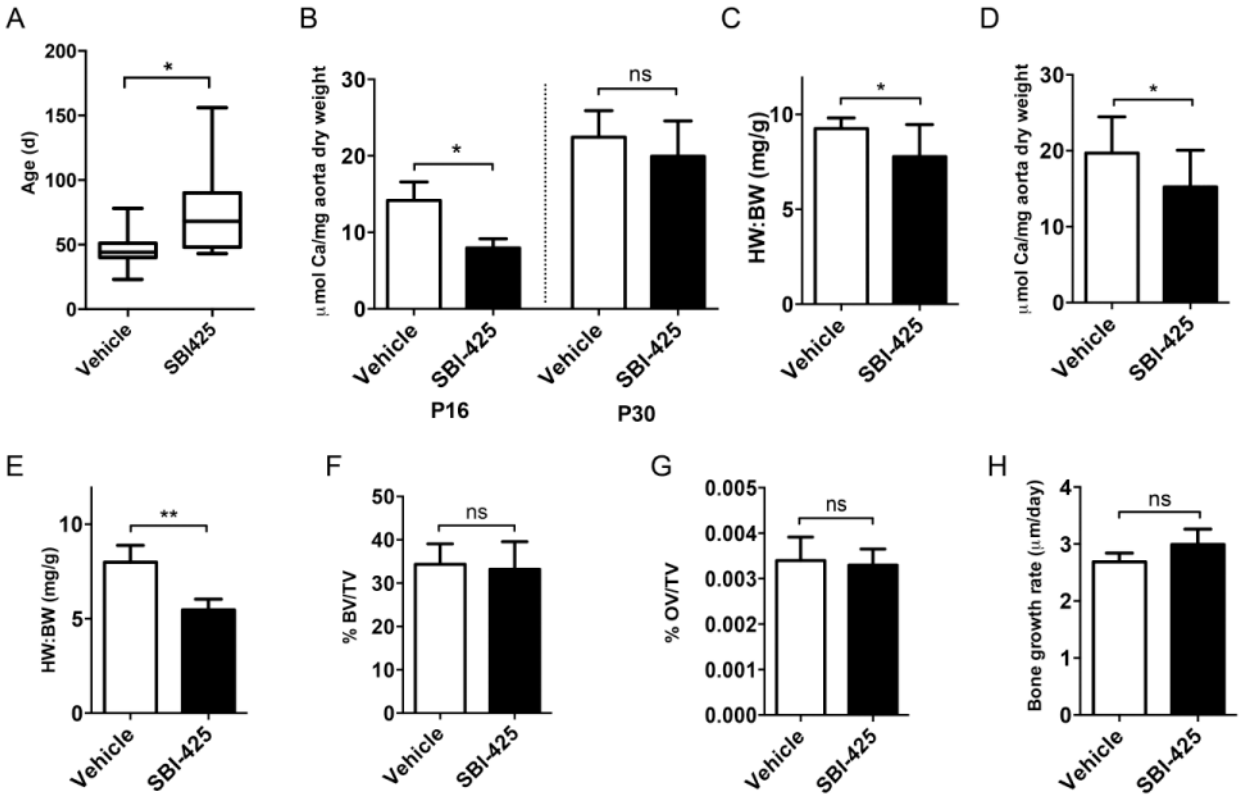

Fig. 6. Efficacy of SBI-425 in TNAP-OE mice and evaluation of effects in bone

(A) Survival analysis of TNAP-OE mice treated with vehicle or SBI-425 from P7 until death. Mann-Whitney U test was used to compare the age of death of mice treated by SBI-425 and Vehicle (exact $p<0.05$). The Hodges-Lehmann estimate of the median difference of age of death of the two groups of mice is 22 days with 95% confidence interval of 4-45. **(B)** Aortic calcium deposition in male TNAP-OE mice treated with vehicle or SBI-425 from P7 to P16 (left side) or P30 (right side). Mice treated with SBI-425 display significantly less aortic calcification than vehicle treated mice at P16, but not at P30 (*N*=4 for mice treated to P16, and *N*=8 and 9 for vehicle- and SBI-425-treated mice, respectively, at P30). **(C)** Heart weight:body weight ratio (HW:BW) in male TNAP-OE mice treated from P7 to P30. Treated male TNAP-OE mice display less cardiac hypertrophy at P30 (*N*=8 and 9 for vehicle- and SBI-425-treated mice, respectively, at P30). **(D)** Aortic calcium deposition and **(E)** HW:BW in double heterozygous $Hprt^{ALPL/Y}$; $Tagln\text{-}Cre^{+/-}$ female mice treated with vehicle or SBI-425 from P7 to P60. SBI-425-treated mice have less aortic calcium and less cardiac hypertrophy than their vehicle-treated counterparts at P60 (*N*=12 and 15 for the vehicle- and SBI-425-treated groups, respectively). **(F)** Bone volume in $Hprt^{ALPL/Y}$; $Tagln\text{-}Cre^{+/-}$ female TNAP-OE treated with vehicle or 10 mg/kg SBI-425 from P7 to P60 measured by histomorphometry of femurs. SBI-425 has no significant effect on bone volume. %BV/TV denotes bone volume as a percentage of total volume (*N*=5). **(G)** Osteoid volume in $Hprt^{ALPL/Y}$; $Tagln\text{-}Cre^{+/-}$ female TNAP-OE mice treated with vehicle or 10

mg/kg SBI-425 from P7 to P60 measured by histomorphometry of femurs. Osteoid volume was not significantly different in female TNAP-OE mice treated with vehicle or SBI-425 (*N*=5). %OV/TV denotes osteoid volume as a percentage of total volume. **(H)** Bone growth rate in male TNAP-OE mice treated with vehicle or SBI-425 from P7 to P30 measured by Alizarin red/calcein chase. SBI-425 has no significant effect on bone growth rate (*N*=5). ns, * and ** denote $P>0.05$, $P<0.05$ and $P<0.01$ by two-tailed Mann-Whitney test. SBI-425 was administered once daily by intraperitoneal injection at 10 mg/kg in all studies.

Table 1
Plasma parameters of male TNAP-OE and WT mice

Age (d)	**14**		**30**	
Genotype	**WT**	**TNAP-OE**	**WT**	**TNAP-OE**
Phosphorus (mg/dL)	12.5 ± 1.0	12.0 ± 1.0	9.1 ± 1.1	9.8 ± 0.2
Calcium (mg/dL)	11.6 ± 0.6	11.5 ± 0.8	10.6 ± 0.7	10.6 ± 1.8
BUN (mmol/L)	12 ± 4.0	12 ± 2.0	15 ± 6.0	17 ± 1.4
ALP (U/L)	541 ± 74.3	2111 ± 199*	197 ± 12.9	3514 ± 1581*
PP_i (pg/mL)	12.8 ± 3.7	13.7 ± 3.6	12.2 ± 7.2	11.3 ± 10.5

BUN, blood urea nitrogen; ALP, alkaline phosphatase; PP_i, pyrophosphate;

* denote different from WT with $P<0.001$, respectively, by two-tailed t-test. $N\geq4$ per group.

Table 2

Fold changes in mRNA expression of calcification-associated genes in TNAP-OE mice.

Age	P14	P30
Gene	**Fold change**	
Alpl	3.00 ± 1.07**	2.90 ± 0.60*
Spp1	18400 ± 9950**	63700 ± 39700**
Bmp2	5.771 ± .39**	12.59 ± 5.54**
Mgp	74.6 ± 49.6**	153.6 ± 65.5**
Col1a1	1.19 ± 0.26	3.43 ± 1.04*
Runx2	9.61 ± 2.35**	7.53 ± 5.56**
Acan	3.16 ± 2.04	17.45 ± 3.30**
Sox9	5.36 ± 2.39*	13.56 ± 7.67*
Phospho1	1.32 ± 0.20	2.22 ± 0.91
Enpp1	2.39 ± 0.62	3.92 ± 0.22**
Ank	3.08 ± 0.23	7.01 ± 6.39
Slc20a1	2.63 ± 0.84*	5.68 ± 2.20*
Acta2	1.04 ± 0.17	0.22 ± 0.11*
Tagln	0.88 ± 0.03	0.38 ± 0.18*

* and

** denote $P<0.05$ and $P<0.01$ by two-tailed t-test, data represent fold change in expression of RNA in TNAP-OE mice relative to WT. $N=3$.

Table 3

Cardiac parameters of P21 male TNAP-OE mice measured by M-mode echocardiography.

Genotype	WT	TNAP-OE
Body weight (g)	12.9 ± 3.4	16.7 ± 1.2
Heart rate (beats/min)	622 ± 92.8	612 ± 40.6
LVMI (mg/g)	3.16 ± 0.40	7.76 ± 0.22***
LVPWd (mm)	0.62 ± 0.04	1.02 ± 0.07***
LVPWs (mm)	1.13 ± 0.10	1.35 ± 0.22
IVSd (mm)	0.64 ± 0.05	1.09 ± 0.13***
IVSs (mm)	1.07 ± 0.10	1.49 ± 0.14***
RWT (mm)	0.43 ± 0.03	0.76 ± 0.06***
EDV (μl)	24.5 ± 4.9	25.6 ± 2.6
ESV (μl)	7.8 ± 1.8	9.5 ± 2.3
LVIDd (mm)	2.98 ± 0.15	2.78 ± 0.30
LVIDs (mm)	1.47 ± 0.30	1.53 ± 0.09
EF (%)	69.6 ± 4.5	61.4 ± 4.7**
FS (%)	51.0 ± 7.4	44.6 ± 5.2
SV (μl)	17.8 ± 1.4	15.0 ± 3.2
CO (mL/min)	11.1 ± 1.2	9.2 ± 2.5

LVMI, Left Ventricular Mass Index; LVPWd, Left Ventricular Posterior Wall Thickness at Diastole; LVPWs, Left Ventricular Posterior Wall Thickness at Systole; IVSd, Interventricular Septal Thickness at Diastole; IVSs, Interventricular Septal Thickness at Systole; EDV, End Diastolic Volume; ESV, End Systolic Volume; Relative Wall Thickness (mm); LVIDd, Left Ventricular Internal Dimension at Diastole; LVIDs, Left Ventricular Internal Dimension at Systole; EF, Ejection Fraction; FS, Fractional Shortening; SV, Stroke volume; CO, Cardiac output.

*
,

**
and

***
denote different from WT with $P<0.05$, $P<0.01$ and $P<0.001$, respectively, by two-tailed t-test. $N=5$ per group.

Table 4

Cardiac parameters of WT and female TNAP-OE mice measured by M-mode echocardiography at 28 and 56 postnatal days.

Age (d)	**28**		**56**	
Sex	**F**		**F**	
Genotype	**WT**	**TNAP-OE**	**WT**	**TNAP-OE**
n	**6**	**9**	**5**	**9**
Parameter				
LVMI (mg/g)	3.73 ± 0.29	5.54 ± 0.67***	3.66 ± 0.31	5.49 ± 0.67***
LVPWd (mm)	0.57 ± 0.06	0.76 ± 0.11**	0.60 ± 0.04	0.88 ± 0.15**
LVPWs (mm)	0.98 ± 0.06	1.15 ± 0.16	1.05 ± 0.28	1.25 ± 0.28
IVSd (mm)	0.59 ± 0.04	0.84 ± 0.08***	0.62 ± 0.04	0.97 ± 0.14***
IVSs (mm)	0.80 ± 0.01	1.23 ± 0.06**	1.04 ± 0.04	1.31 ± 0.28*
RWT (mm)	0.37 ± 0.03	0.56 ± 0.05***	0.36 ± 0.01	0.62 ± 0.12***
EDV (μl)	25.9 ± 2.4	24.0 ± 4.2	31.8 ± 2.9	28.5 ± 6.5
ESV (μl)	7.5 ± 1.1	7.2 ± 1.2	9.2 ± 1.3	9.7 ± 3.6
LVIDd (mm)	3.16 ± 0.11	2.88 ± 0.22*	3.43 ± 0.20	3.03 ± 0.27*
LVIDs (mm)	1.70 ± 0.09	1.43 ± 0.19	1.87 ± 0.16	1.59 ± 0.42
EF (%)	71.1 ± 2.6	69.9 ± 2.7	71.2 ± 2.9	66.6 ± 4.8
FS (%)	45.0 ± 3.6	50.2 ± 5.8	45.6 ± 2.0	48.1 ± 10.0

LVMI, Left Ventricular Mass Index; LVPWd, Left Ventricular Posterior Wall Thickness at Diastole; LVPWs, Left Ventricular Posterior Wall Thickness at Systole; IVSd, Interventricular Septum Distance at Diastole; IVSs, Interventricular Septum Distance at Systole; EDV, End Diastolic Volume; ESV, End Systolic Volume; Relative Wall Thickness (mm); LVIDd, Left Ventricular Internal Dimension at Diastole; LVIDs, Left Ventricular Internal Dimension at Systole; EF, Ejection Fraction; FS, Fractional Shortening.

*, **and ***denote different from WT with $p<0.05$, $p<0.01$ and $p<0.001$, respectively, by two-tailed t-test.